Indian Journal of Pure & Applied Physics
Vol. 64, February 2026, pp. 167-180
DOI: 10.56042/ijpap.v64i2.25704

A Mathematical and Simulation Study of Lanthanum-Modified PZT for Enhanced Serendipity Shaped Cantilever Piezoelectric Energy Harvester

Hemant Narayan[a], Prakash Marimuthu[a]*, Shakila Baskaran[a] & Kumar Rajagopal[b]

[a]Department of Electrical and Electronics Engineering, National Institute of Technology Nagaland 797 103, India

[b]Department of Electronics and Instrumentation Engineering, National Institute of Technology Nagaland 797 103, India

Received: 19th November 2025; accepted: 29th December 2025

Piezoelectric energy harvesting is widely explored for powering low-frequency structural-health-monitoring (SHM) systems. The effect of lanthanum (La) mixing on the performance of PZT-5A and PZT-5J, particularly in nonuniform cantilever geometries, remains insufficiently explored. In this work, the effect of La concentrations of 1.12, 2.24, and 3.36 percentage of weights in a serendipity shaped cantilever piezoelectric energy harvester were examined using copper, silicon, and structural-steel substrates with nickel electrodes. A reduced single-degree-of-freedom electromechanical model was developed to interpret the simulated behaviour. Results show that La mixing enhances output voltage and harvested power across all configurations. The highest performance was obtained for PZT-5A with structural steel and 3.36 % La, yielding 15.47 V and 9.98 mW at 32 Hz. For PZT-5J with 3.36 % La on copper, 13.466 V and 7.55 mW were achieved. Analytical calculations predicted a maximum power of 9.319 mW at an optimal load of 50 kΩ. Capacitance of 96.2 nF for PZT-5A and 107.5 nF for PZT-5J corresponded to electrical reactance near 51.7 kΩ and 46.3 kΩ. An extraction efficiency of 26.1 % under 2 g excitation was estimated. Overall, La mixing improved the output by 12–13 %, providing an effective design pathway for enhanced PZT-based energy harvesters for low-frequency SHM applications.

Keywords: Energy harvester, Piezoelectric, Lanthanum, Nickel, PZT-5A, PZT-5J

1 Introduction

Over the last decade, there has been a significant rise in the development and implementation of energy-harvesting technologies that focus on providing continuous power for low-power electronic devices. These methods are becoming more prevalent in wireless data transmission, sensing, actuation, and healthcare monitoring systems. In this context, there has been a lot of research into improving the performance of piezoelectric materials, which can transform mechanical vibrations into electrical energy and vice versa. According to research, the majority of ambient vibration sources of practical interest are at low frequencies, often less than 200 Hz. Piezoelectric energy harvesters (PEHs) are ideal for such situations due to their high power density, simple structural design, and ease of integration[1,2]. Among available piezoelectric ceramics, PZT-5A and PZT-5J are widely used because of their high piezoelectric coefficients, thermal stability, mechanical robustness, and cost-effectiveness. The present work focuses on improving their electromechanical performance through lanthanum mixing.

Lanthanum mixing has been extensively explored in various piezoelectric materials to enhance their energy harvesting performance. In ZnO-based Nano generators, La doping in the range of 0–7.5% has been optimized, with contents above 2.5 % yielding a three- to four-fold increase in output[3]. Lanthanum-doped barium stannate, a refractory near-zero-index material, has demonstrated strong potential for near-infrared thermal emission and has shown thermal stability at temperatures exceeding 1000 ℃[4]. Similarly, Nano-sized lanthanum-modified bismuth titanate (BLT) powders prepared via high-speed ball milling have exhibited more than four times the harvested energy compared to their micro-sized counterparts[5]. ZnO nanorods doped with lanthanum have also been reported to produce nearly three times the output of intrinsic piezoelectric nanogenerators[6]. In addition, piezoelectric energy-harvesting systems have been integrated into building envelopes to power fiber-grating sensors, enabling continuous structural-health monitoring[7]. Studies on perforated rectangular cantilevers have further shown increased power extraction from wind and structural vibrations, supporting applications in wireless monitoring frameworks[8]. Flexible composite systems such as

*Corresponding author: E-mail: prakash13688@gmail.com

PVDF/La-based oxides[9,10] and Pr-doped $La_2Ti_2O_7$ films[11] successfully achieve measurable electrical power output in the μW–mW range under low-frequency mechanical excitation, highlighting their suitability for energy harvesting. In contrast, bulk La-modified ceramics including BNKT-ST, $BiFeO_3$, and $PbTiO_3$ primarily focus on enhancing dielectric constant[12], ferroelectric stability, Curie temperature[13], and domain behaviour[14] rather than power generation. PLZT systems[15] exploit La doping to balance transparency and piezoelectricity for actuation and acoustic applications. Overall, these works reveal a clear gap between La-enhanced ferroelectric optimization and efficient vibration-based energy harvesting, motivating further research on La-doped harvesters.

The lanthanum concentration ranges of 1.12–3.36 wt % was selected based on literature regarding material stability limits, piezoelectric performance trends, and practical fabrication considerations. Low-concentration of La mixing serves as a donor dopant in PZT ceramics, improving dielectric permittivity and domain wall mobility while reducing oxygen vacancy formation. However, La concentrations greater than 4 wt % will result in significant dielectric loss, reduced mechanical stiffness, and increased brittleness, which are undesirable for energy harvesting applications.

According to current study, La concentration ranges of 1.12 to 3.36 wt % increases the output voltage and harvested power at an average of 12-13 %, achieved using PZT-5A and PZT-5J ceramics in a low-frequency range (32 Hz). This improvement in output helps in low-frequency PZT-based energy harvesting devices, demonstrating the effectiveness of controlled La mixing combined with optimized device geometry.

Lightweight PZT-based composite structures have been employed in the aerospace industry for energy harvesting and structural-health monitoring, particularly under axial airflow and harsh environmental conditions where continuous power is required[16]. In such applications, PZT patches have been shown to outperform circular piezoelectric elements. Studies on PZT ceramics with varying Zr/Ti ratios (36/64–68/32) have reported significant differences in functional properties, including band gap, energy-storage density, and permittivity, with the highest energy density of 172.23 mJ/cm³ observed for the 36/64 composition at 200 ℃[17]. High piezoelectric output voltage up to 3.45 *V* have also been achieved using p-type ZnO nanowires doped with group-V elements (P, As, Sb), where reduced leakage currents and improved polarization contribute to enhanced performances[18]. Additional research has shown that ZnO nanowire transducers exposed to CO_2 exhibit increased output voltages (up to 1.795 V) due to surface redox reactions, with voltage saturation occurring after two hours of exposure at 20 ppm[19]. Emerging materials such as perovskites and polymers help in increasing high scalability and power density, making them suitable for self-powered sensors and transducers[20,21]. As the growing demand of IoT systems, energy harvesting from ambient vibrations and electromagnetic fields using piezoelectric materials and polymers offers a sustainable solution that reduces battery dependency and increases device durability[22,23].

Despite substantial improvements in piezoelectric energy harvesting, there is still a research gap remaining in how La mixing affects the electromechanical coupling for PZT-5A and PZT-5, when implemented in non-uniform geometries such as serendipity-shaped cantilever beams. Previous research has generally focused on La doping in ZnO, BLT, PZT etc., comparison in different La concentrations and substrate materials are largely absent. Furthermore, current research often integrates finite-element simulations with an analytically derived single-degree-of-freedom (SDOF) electromechanical model to obtain optimal electrical loading, damping behaviour, and harvested power.

The present work addresses these gaps by performing a thorough investigation of La-mixed PZT-5A and PZT-5J using COMSOL Multiphysics, using a reduced-order electromechanical model for validation. The study provides quantitative analysis for multiple La concentrations, substrate materials, and electrical loading conditions that provide enhanced output voltage, power generation, electromechanical coupling, capacitance, reactance, and efficiency. The findings demonstrate that La mixing leads to a 12–13 % enhancement in output performance, and the combined simulation–analytical approach offers a practical design pathway for optimizing PZT-based energy harvesters intended for low-frequency structural health monitoring applications.

2 Dynamic Modelling and Device Configuration

Finite element modelling (FEM) used to predict the electromechanical response of piezoelectric harvesters but offers limited analytical insight into damping, resonance, and load optimization. Therefore, a reduced-

order single-degree-of-freedom electrome-chanical model[16] as mentioned in Eq. (1) is employed to complement FEM, enabling efficient interpretation, validation, and design optimization of the proposed energy harvester.

2.1 Dynamic Modelling

The energy harvester proposed in this article consists of a cantilever beam with an effective mass m_{eff} having unit in kg, mass density ρ with unit kg/m^2, having cross-sectional area $\mathcal{A}$ with unit m^2, $\mathcal{L}$ beam length having unit in m, $\mathcal{V}(\mathrm{t})$ Electrical potential difference with unit V that develops as the piezo is strained means open circuit, Electric field $\mathcal{E}$ with unit V/m, c_{m} mechanical damping and single mode amplitude displacement $\mathrm{D}(t)$ having unit m. Excitation force $\mathrm{f_{ext}}(\mathrm{x},\mathrm{t})$ having unit N/m is driven by external force, piezoelectric material of thickness $\hbar_p$ having unit in m. The negative sign indicates that the excitation force acts opposite to the direction of beam displacement.

$$\mathrm{m_{eff}}\frac{\mathrm{d}^2\mathrm{D}(t)}{\mathrm{d}t^2}+c_{\mathrm{m}}\frac{\mathrm{dD}(t)}{\mathrm{d}t}+\hbar_{\mathrm{eff}}\mathrm{D}(t)+\xi\mathcal{V}(t)=-\mathrm{f_{ext}}(t) \quad \ldots (1)$$

ξ is electromechanical transduction coefficient having unit C/m, $\mathrm{f_{ext}}(t)$ is external applied inertial force when cantilever beam is in motion with acceleration $\mathrm{a_m}(t)$ having unit m/s^2 shown in Eq. (2).

2.1.1 External Excitation and Natural Frequency

The external excitation acting on the cantilever is expressed as an inertial force induced by base acceleration. This formulation relates the applied acceleration to the effective mass of the system.

$$f_{ext}(t)=m_{eff}a_m(t) \quad \ldots (2)$$

i. Natural Frequency (ω_n)

The natural frequency with unit rad/s of the system is determined by the beam's stiffness $\hbar_{eff}$ having unit N/m of cantilever beam as shown in Eq. (3).

$$\omega_n=\sqrt{\frac{\hbar_{eff}}{m_{eff}}} \text{ or } \hbar_{eff}=m_{eff}{\omega_n}^2 \quad \ldots (3)$$

ii. Electromechanical coupling (K^2)

Electromechanical coupling coefficient as mentioned in Eq. (4) is dimensionless quantity and have range 0 to 1. It represents fraction of stored mechanical energy that can be converted to electrical energy in one cycle.

$$K^2=\frac{\xi^2}{\hbar_{eff}c_p} \quad \ldots (4)$$

For a purely resistive electrical load direc

iii. Electrical circuit equation

Electrical circuit equation when resistive load $\mathcal{R}$ having unit Ω, $q(t)$ Electric charge with unit C accumulated on the electrodes[24] as shown in Eq (5).

$$q(t)=\xi d(t)+c_p\mathcal{V}(t) \quad \ldots (5)$$

tly across the piezo, the circuit equation is simplified to express the relationship between voltage, current, resistance and piezo capacitance as shown in Eq (6).

$$c_p\frac{d\mathcal{V}(t)}{dt}+\frac{\mathcal{V}(t)}{\mathcal{R}}+\xi\frac{dD(t)}{dt}=0 \quad \ldots (6)$$

$\xi\frac{dD(t)}{dt}$ is piezo generated current and $c_p\frac{d\mathcal{V}(t)}{dt}$ is current through capacitor having units A. The piezo-generated charge (mechanical contribution) comes from the constitutive relation[25] (strain-charge form)

$$\mathcal{D}(t)=e_{31}\mathcal{S}(t)+\in_{33}\mathcal{E}(t) \quad \ldots (7)$$

where electric displacement $\mathcal{D}(t)$ having unit C/m², e_{31} piezoelectric stress constant C/m², $\mathcal{S}$ axial strain in the piezo layer, which is a dimensionless, permittivity of the piezoelectric material $\in_{33}$ with unit F/m as mentioned in Eq. (7).

2.1.2 Damping Mechanisms

i. Mechanical Damping (ζ_m)

It represents the energy lost due to internal and external mechanical resistance in the vibrating structure. ζ_m is mechanical damping force per unit length and is proportional to velocity of vibrating beam as shown in Eq. (8).

$$\zeta_m=\frac{\mathscr{b}_m}{2m_{eff}\omega_n} \quad \ldots (8)$$

The mechanical damping force, $f_{mech}(t)=\mathscr{b}_m\frac{dD(t)}{dt}$ is expressed as velocity proportional term, representing distributed viscous damping along the beam length.

$$\mathscr{b}_m=\int_0^{\mathcal{L}}c_m(x)D^2(x)dx \quad \ldots (9)$$

where $\mathscr{b}_m$is equivalent mechanical damping coefficient with unit Ns/m, $c_m(x)$ is mechanical damping coefficient per unit length having unit Ns/m^2 as mentioned in Eq. (9), representing distributed

viscous-type damping from internal friction, material losses, or mounting losses. It reduces the vibration amplitude and dissipates energy as heat. It causes internal friction and material losses.

ii. Electrical Damping (ζ_e)

It is the energy extracted from the system due to electrical energy conversion in the piezoelectric material. ζ_e is electrical damping force per unit length and is proportional to velocity of vibrating structure as shown in Eq. (10). It occurs when the piezoelectric element is connected to a load.

$$\zeta_e = \frac{\mathscr{b}_e}{2m_{eff}w_n} \quad \ldots (10)$$

The electrical damping force, $f_{elect}(t) = \mathscr{b}_e \frac{dD(t)}{dt}$

In the frequency domain the effective additional mechanical damping contributed by the electrical circuit is

$$\mathscr{b}_e(w) = \frac{\xi^2 \mathcal{R}}{1+(w_n c_p \mathcal{R})^2} \quad \ldots (11)$$

where $\mathscr{b}_e$ is electrical damping coefficient and $\mathscr{b}_e(w)$ is frequency dependent electrical damping with unit Ns/m, ξ is the electromechanical coupling coefficient, relates mechanical displacement of the beam to generated charge. c_p is the piezo capacitance with unit F as mentioned above in Eq. (11). Too much electrical damping reduces piezoelectric output, and which affects output power.

iii. Air Damping (ζ_a)

It refers to resistance force exerted by the output, surrounding air on the vibrating cantilever beam. It causes energy dissipation, reducing the amplitude of oscillations. ζ_a is air damping force per unit length and is proportional to velocity of the beam as shown in Eq. (12). This is represented as

$$\zeta_a = c_a(x) \frac{dD(x,t)}{dt} \quad \ldots (12)$$

The air damping force, $f_{air}(t) = c_a \frac{dD(t)}{dt}$

$$c_a = \int_0^{\mathcal{L}} c_a(x) D^2(x) dx \quad \ldots (13)$$

where c_a is the air damping coefficient Ns/m and $D^2(x)$ is the displacement in x axis, as shown above in Eq. (13).

iv. Total Damping (ζ_{Total})

The total damping ratio of the system is obtained by combining mechanical, electrical, and air damping contributions to describe the overall energy dissipation mechanism, as calculated in Eqs (14-16).

$$\zeta_{Total} = \zeta_m + \zeta_e + \zeta_a \quad \ldots (14)$$

$$\zeta_{Total} = \frac{c_{eff}}{2m_{eff}w_n} \quad \ldots (15)$$

$$\text{And } c_{eff} = \mathscr{b}_m + \mathscr{b}_e(w) + c_a \quad \ldots (16)$$

v. Final Combined Dynamic Equation with Damping

By coupling the mechanical dynamics with the electrical circuit equations and damping effects, the final governing equation of the piezoelectric energy harvester is obtained in Eq. (17).

$$m_{eff}\frac{d^2D(t)}{dt^2} + c_{eff}\frac{dD(t)}{dt} + \mathscr{k}_{eff}D(t) + \xi\mathcal{V}(t) = -f_{ext}(t) \quad \ldots (17)$$

2.1.3 Frequency Response and Resonance

The external excitation is assumed to be sinusoidal base acceleration, which induces an inertial force on the cantilever beam. No prescribed displacement or oscillatory motion is imposed directly on the structure. Assuming the excitation force $f_{ext}(x,t)$ is harmonic in time, $\mathcal{F}(x)$ spatial distribution, as shown in Eq. (18). The system response is calculated from Eqs. (19-23), using phasor representation to obtain steady-state displacement, voltage, and phase relationships.

$$f_{ext}(x,t) = \mathcal{F}(x)\cos(wt) \quad \ldots (18)$$

The system response has an angular frequency w, $\emptyset$ denotes phase shift depending on damping, $\mathcal{F}_o$ is force amplitude corresponding to the first vibration mode with unit N, $D(t)$ modal displacement and $\mathcal{V}(t)$ across piezoelectric layer, and equation shown below:

$$D(t) = Real(\hat{D}e^{jwt}) \text{ and } \mathcal{V}(t) = Real(\hat{\mathcal{V}}e^{jwt}) \quad \ldots (19)$$

In time domain, steady-state displacement of the beam is:

$$D(t) = \left|\hat{D}\right|\cos(wt - \emptyset) \quad \ldots (20)$$

The amplitude of the displacement is given by:

$$\left|\hat{D}(w)\right| = \frac{\frac{\mathcal{F}_o}{m_{eff}}}{\sqrt{({w_n}^2 - w^2)^2 + (2\zeta_{Total}w_n w)^2}} \quad \ldots (21)$$

$$F_m^{ext}(x,t) = \left(\int_0^{\mathcal{L}} D(x)\mathcal{F}(x)dx\right)\cos(\omega t) = \mathcal{F}_o\cos(\omega t) \quad \ldots (22)$$

$$\mathcal{F}_o = \int_0^{\mathcal{L}} D(x)\mathcal{F}(x)dx \quad \ldots (23)$$

i. Resonance Condition

The harvested power is maximized when the excitation frequency matches the system's natural frequency ($\omega = \omega_n$). At resonance, the amplitude of displacement is maximized, as shown in below Eq. (24).

$$\left|\hat{D}(\omega)\right| = \frac{\frac{\mathcal{F}_o}{m_{eff}}}{2\zeta_{Total}\omega_n} \quad \ldots (24)$$

ii. Electrical Power Output

The electrical power $\mathcal{P}_e$ harvested by the electrical damper is proportional to the velocity mean squared $\left(\frac{dD(t)}{dt}\right)^2$ calculated in Eqs. (25-29) with efficiency.

$$\text{Average}\left(\frac{dD(t)}{dt}\right)^2 = 0.5\left(\omega\left|\hat{D}\right|\right)^2 \quad \ldots (25)$$

$$\mathcal{P}_e = \mathcal{b}_e(\omega)0.5\left(\omega\left|\hat{D}\right|\right)^2 \quad \ldots (26)$$

$$\text{At resonance, } \mathcal{b}_e(\omega_n) = 2m_{eff}\omega_n\zeta_e \quad \ldots (27)$$

The maximum harvested power is

$$\mathcal{P}_{e,max} = \frac{\frac{\mathcal{F}_o{}^2}{m_{eff}}}{16\zeta_{Total}\omega_n}\frac{\zeta_e}{\zeta_{Total}} \quad \ldots (28)$$

Hence, $\mathcal{P}_e$ is directly proportional to $\frac{\frac{\mathcal{F}_o{}^2}{m_{eff}}}{16\zeta_{Total}\omega_n}$ only if $\zeta_e = \zeta_{Total}/2$, means the maximum harvested power is obtained when electrical damping is equal to mechanical damping ($\zeta_e = \zeta_m$), which corresponds to the maximum power transfer theorem for piezoelectric systems. This condition defines the electrical impedance of the load effectively matches the internal electromechanical impedance of the harvester, resulting in the optimal energy transfer from the mechanical to electrical circuit with optimal load resistance of 50 KΩ, the system efficiency is defined as

$$\eta = \frac{\zeta_e}{\zeta_m+\zeta_e+\zeta_a} \quad \ldots (29)$$

2.2 Device configuration

To perform comparative simulation and analysis, a seismic mass was bonded to the top surface at the free end of the proposed cantilever beam, while the opposite end was rigidly fixed to the excitation platform using appropriate boundary constraints. The seismic mass, with dimensions of 4 × 9.92 × 1 mm, corresponds to a physical mass of 0.311 gram. Figure 1 illustrates the structural configuration of the serendipity-shaped cantilever-based MEMS piezoelectric vibration energy harvester (PVEH), including the chamfered seismic mass. The device geometry was incorporated by chamfer to reduce stress concentration at the free end near seismic mass and to ensure smooth geometric configuration along the piezoelectric beam. The detailed geometrical parameters are provided in Table 1.

Free-triangular elements were used to perform Finite element analysis (FEA). The meshing with a maximum element size of 6.99 mm, a minimum element size of 0.006 mm, a maximum element growth rate of 1.5, and a curvature factor of 0.6, ensuring high mesh quality and reliable simulation results across the computational domain.

The proposed cantilever shape promotes more uniform strain distribution over traditional rectangular cantilever geometries. The highest strain in rectangular

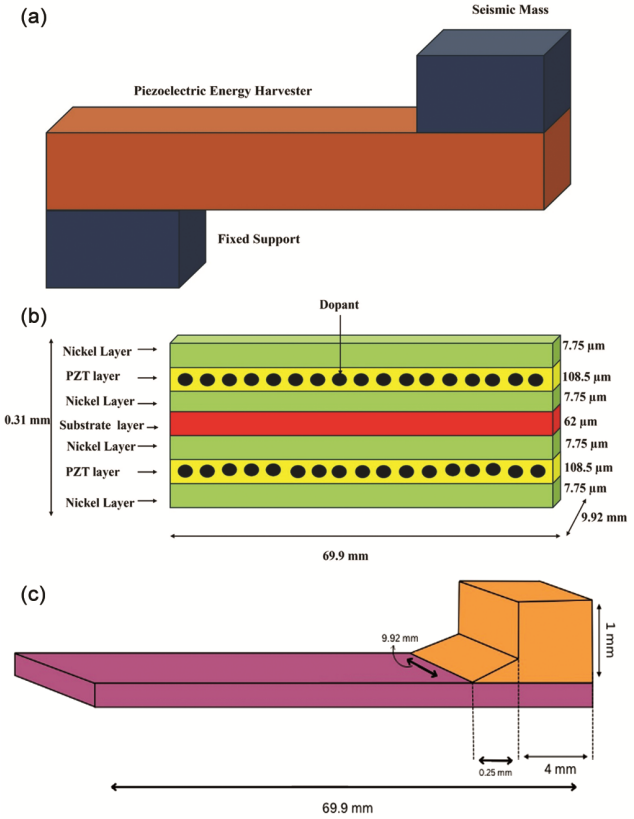

Fig. 1 — (a) Proposed Piezoelectric Energy Harvester (b) Dimensions with different layers and La mixing (c) Dimensions of Seismic Mass with chamfer

Table 1 — Dimensions of serendipity cantilever beam PVEH

Parameter	Piezoelectric Material		Substrate			Layer (Nickel)	La
	PZT-5A	PZT-5J	Cu	Si	Str Steel		
Length (*mm*)	69.9	69.9	69.9	69.9	69.9	69.9	0.050
Width (*mm*)	9.92	9.92	9.920	9.920	9.920	9.920	9.920
Thick (*mm*)	0.108	0.108	0.062	0.062	0.062	0.007	0.050
Density(*kg/m*3)	7750	7400	8960	2329	7850	8900	6150
Young's (*GPa*)	66	66	120	170	200	219	36
Poisson's ratio	0.31	0.31	0.34	0.28	0.3	0.31	0.28
Permittivity	1700	1900	1	11.7	1	1	1

cantilevers is only near the fixed end, limiting the effective use of the piezoelectric material and perhaps leading to increased stress concentrations. Whereas the proposed serendipity shape piezoelectric energy harvester redistributes bending stress over a longer effective length, lowering peak stress at the clamped region.

3 Characteristics of the Proposed Device

The characteristics of proposed device were evaluated to determine the key electromechanical parameters of the proposed serendipity-shaped piezoelectric energy harvester. The detailed geometric dimensions were mentioned in Table 1. The electrode area was computed as 6.934×10^{-4} m^2. Using the piezoelectric layer dimensions, its volume and mass were obtained as 7.523×10^{-8} m^3 and 5.830×10^{-4} Kg, respectively.

The substrate contributed a volume of 4.299×10^{-8} m^3 and a mass of 3.374×10^{-4} Kg. The seismic mass mounted at the free end was 3.11×10^{-4} Kg, while the two nickel electrode layers contributed an additional 9.565×10^{-5} Kg. The total beam mass, which includes piezoelectric material, substrate, and nickel, was thus calculated as 1.016×10^{-3} Kg. Using the standard modal mass relation for first-mode cantilevers, the effective mass was determined as 5.508×10^{-4} Kg as mentioned in Table 2.

For a resonant frequency of 32 Hz, the corresponding angular frequency was obtained as ω_n= 201.06 rad/s. The modal stiffness was then evaluated 22.267 N/m. The capacitance of the piezoelectric layer was calculated 96.2 nF for PZT-5A and 107.5 nF for PZT-5J. Using these capacitances, the capacitive reactance values at 32 Hz were found to be 51.7 kΩ and 46.3 kΩ, respectively. The electromechanical coupling coefficient ξ, based on geometric and material properties, was estimated as 1.74×10^{-4} C/m.

The maximum harvested electrical power was determined to be 9.319 mW at an optimal load resistance of 50 kΩ. The electrical damping coefficient was computed as 7.80×10^{-4} Ns/m. The total damping ratio of the system, including mechanical, electrical, and air damping contributions, was 0.0135. Under a 2g base excitation, the conversion efficiency at resonance was found to be approximately 26.1 %, confirming strong electromechanical coupling and effective energy extraction from the device.

Table 2 — Calculated parameters for proposed dimensions

S No.	Parameter	Value
1	Electrode Area, A	6.934×10^{-4} m^2
2	Piezoelectric volume, V_{PZT}	7.523×10^{-8} m^3
3	Piezoelectric Mass, M_P	5.830×10^{-4} Kg
4	Substrate volume, V_{sub}	4.299×10^{-8} m^3
5	Substrate Mass, M_{sub}	3.374×10^{-4} Kg
6	Seismic Mass, M_s	3.11×10^{-4} Kg
7	Nickel Mass, M_{Ni} (2 layers)	9.565×10^{-5} Kg
8	Total Beam Mass, M_{TB}	1.016×10^{-3} Kg
9	Total effective mass, m_{eff}	5.508×10^{-4} Kg
10	Modal stiffness, k_{eff}	22.267 N/m
11	Natural frequency, ω_n	201.06 rad/sec
12	Permittivity of free space, ε_0	8.854×10^{-12} F/m
13	Capacitance (PZT-5A), c_p	96.2 nF
14	Capacitance (PZT-5J), c_p	107.5 nF
15	Reactance (PZT-5A), X_c	51.7 KΩ
16	Reactance (PZT-5J), X_c	46.3 KΩ
17	Estimated electromechanical coefficient, ξ	1.74×10^{-4} C/m
18	Electrical Damping, b_e	7.80×10^{-4} Ns/m
19	Total Damping, ζ_{Total}	0.0135
20	Acceleration, g	2

Total Beam Mass (M_{TB}) = Piezoelectric + Substrate + Nickel = $1.016 \times 10^{-3}\,Kg$

Total effective mass, $m_{eff} = 0.236M_{TB} + M_s = 5.508 \times 10^{-4}\,Kg$

The piezoelectric layer capacitance is given by Eq. (30), where ε_r is the relative permittivity and ε_0 is 8.854×10^{-12} F/m,

$$c_p = \frac{\varepsilon_r \varepsilon_0 \mathcal{A}}{h_p} \quad \ldots (30)$$

Capacitance for PZT-5A will be 96.2 nF and for PZT-5J will be 107.5 nF. Capacitive reactance (X_c) at 32 Hz of resonant frequency will be,

$$X_c = \frac{1}{w_n c_p} \quad \ldots (31)$$

Capacitive reactance for PZT-5A and PZT-5J will be 51.7 KΩ and 46.3 KΩ. Estimated ξ electromechanical transduction coefficient is 1.74 × 10^{-4} C/m. Maximum harvested power,

$\mathcal{P}_{e,max}$ = 9.319 mW occurs at 50 KΩ

Hence, the maximum harvested electrical power was analytically predicted to be 9.319 mW at an optimal load resistance of 50 kΩ. Under resonant operation with a base excitation of 2 g, the corresponding energy conversion efficiency was estimated to be approximately 26.1 %, confirming effective electromechanical coupling and efficient vibration-to-electric energy conversion.

4 Simulation Results and Discussion

The potential generation of proposed structure was investigated by using FEM in COMSOL Multiphysics. The simulations were performed to evaluate the electromechanical response of the device, with particular emphasis on output voltage and harvested electrical power under harmonic base excitation. The coupled piezoelectric–structural physics interface was employed to accurately capture the interaction between mechanical deformation and electrical potential generation within the piezoelectric layer.

4.1 Resonance Frequency Dependence

Resonance frequency dependence examines the beam's behaviour with variations in frequency. The study investigated the variation in output voltage and electrical power through varying frequency for different La mixing concentrations ranging from 1.12 wt % to 3.36 wt % in both PZT-5A and PZT-5J materials. Figure 2 demonstrated the simulated voltage and power responses at different frequencies for different La mixing concentration in PZT-5A and PZT-5J. The corresponding simulation results with different substrate materials and lanthanum concentrations are presented in Table 3. A significant rise in output voltage and electric power was observed within the frequency range of 25–35 Hz, demonstrating frequency sensitivity of the proposed design.

The influence of substrate material was also examined by considering copper, silicon, and structural steel substrates. The highest output voltage and electrical power were obtained simultaneously in several device configurations. With 1.12 % lanthanum mixing, PZT-5A with a structural-steel substrate (device 3) produced 15.08 V and 9.485 mW at 32 Hz, while PZT-5J with a copper substrate (device 10) generated 13.2 V and 7.262 mW at the same frequency. When the lanthanum concentration increased to 2.24 %, PZT-5A with structural steel (device 6) yielded 15.41 V and 9.88 mW at 31.5 Hz, whereas PZT-5J with copper (device 13) produced 13.11 V and 7.17 mW at 32 Hz. At the highest mixing level of 3.36 %, PZT-5A with structural steel (device 9) achieved 15.47 V and 9.98 mW at 32 Hz, while PZT-5J with copper (device 16) delivered 13.46 V and 7.55 mW at 32 Hz, where the resonant and excitation frequencies were matched.

However, increasing the frequency from 35 Hz to 80 Hz, there was a drop significantly in both output voltage and power. Therefore, it can be concluded that the optimal operating frequency for the proposed structure in case of PZT – 5A and PZT – 5J is 32 Hz, and the resonant frequency analysis confirms that the proposed serendipity-shaped cantilever design, combined with optimized lanthanum mixing, effectively enhances voltage generation and power output in the low-frequency regime relevant to structural health monitoring applications.

4.2 Load Resistance Dependence

The effect of load resistance on the beam's performance at the resonant frequency of 31.5 Hz was investigated. Table 4 shows simulated results, and the graphical representation is shown in Fig. 3. As the load resistance was increased, both the output voltage and output power initially increased, with maximum values observed near the optimal resistance range. However, when the load resistance exceeded 100 kΩ, the harvested power decreased almost linearly, while the voltage continued to increase at a slower rate. This behaviour of piezoelectric energy harvesters operating under resistive loading, where high load resistance limits current flow and consequently reduces power transfer.

Electromechanical coupling losses were employed to ensure accurate representation of the device's behaviour under varying electrical loads. The simulated results in load dependence are consistent with the analytical SDOF model and the maximum

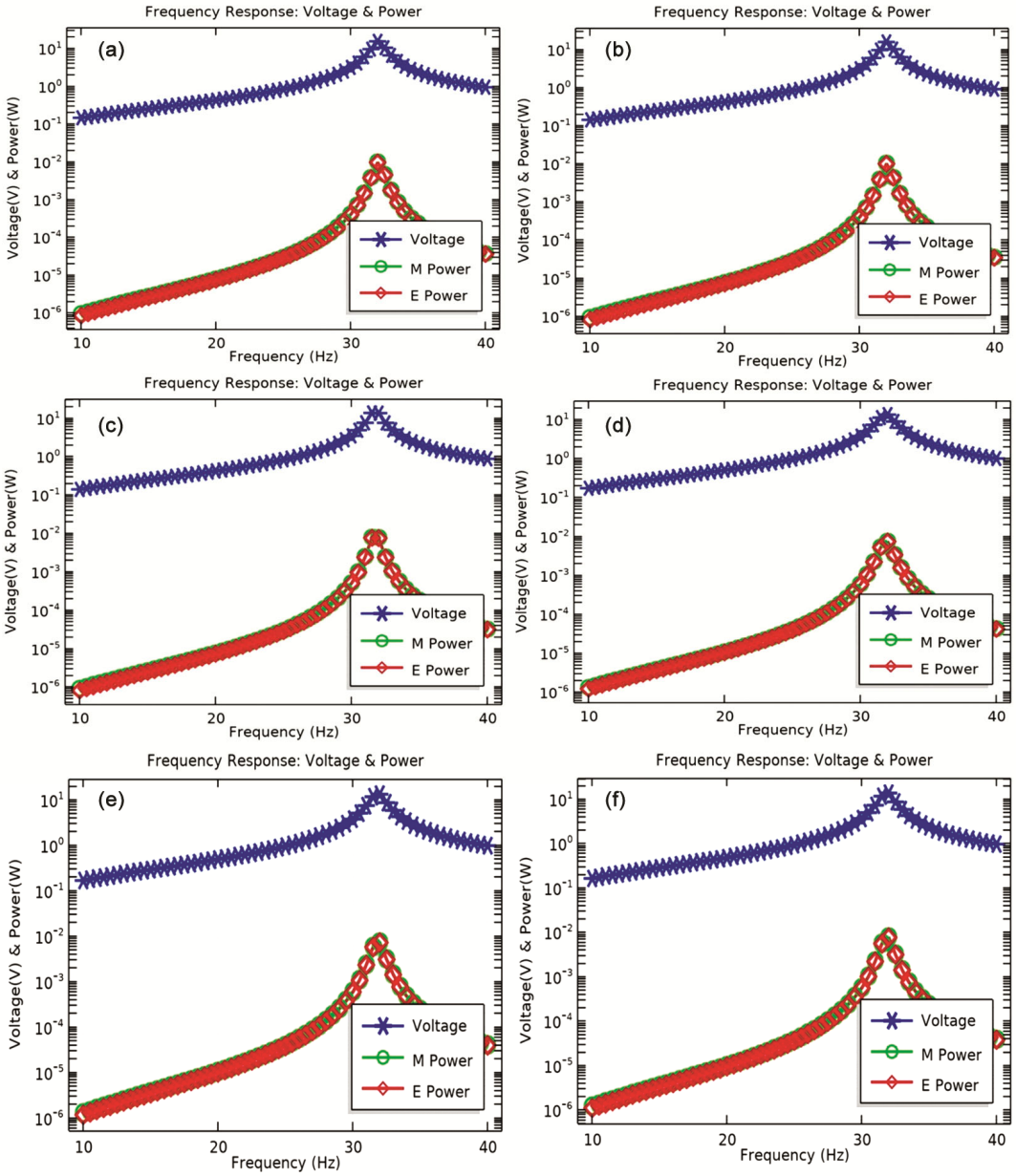

Fig. 2 — Frequency Response of devices: In case of PZT -5A with structural steel (a) Device 3 (1.12 % lanthanum) (b) Device 6 (2.24 % lanthanum) (c) Device 9 (3.36 % lanthanum). In case of PZT-5J with copper (d) Device 10 (1.12 % lanthanum) (e) Device 13 (2.24 % lanthanum) and (f) Device 16 (3.36 % lanthanum)

power transfer condition, validating the numerical approach and the effectiveness of the proposed device design.

4.3 Acceleration Dependence

Simulations were conducted at the resonant frequency to evaluate the output voltage and electrical power for varying acceleration ranging from 0 to 2 g. The results, illustrated in Fig. 4, revealed a relationship between acceleration and output electrical power. Both the output voltage and harvested power exhibited a monotonic rise as the applied acceleration increases, indicating increased strain-induced charge generation within the piezoelectric layer. This behaviour is consistent with the linear vibration range, where the inertial force acting on the cantilever increases proportionally with acceleration, leading to higher mechanical deformation and electrical response. At resonant frequency 31.5 Hz, device operates in a stable linear range without stiffness or hardening effects.

Table 3 — COMSOL Simulated Results in Frequency response

			Frequency Response			
Device	Material		La Mixing (%)	Voltage (*V*)	Power (*mW*)	Frequency (*Hz*)
1	PZT-5A	Cu	1.12	13.86	8.004	31.5
2		Si	1.12	13.38	7.469	33.5
3		Str Steel	1.12	15.08	9.485	32
4	PZT-5A	Cu	2.24	14.24	8.451	31.5
5		Si	2.24	13.49	7.582	33.5
6		Str Steel	2.24	15.42	9.881	31.5
7	PZT-5A	Cu	3.36	13.45	7.851	31.5
8		Si	3.36	14.14	8.334	33.5
9		Str Steel	3.36	15.47	9.983	32
10	PZT-5J	Cu	1.12	13.22	7.262	32
11		Si	1.12	11.82	5.874	33.5
12		Str Steel	1.12	12.52	6.536	32
13	PZT-5J	Cu	2.24	13.11	7.171	32
14		Si	2.24	12.22	6.222	33.5
15		Str Steel	2.24	13.00	7.046	32
16	PZT-5J	Cu	3.36	13.46	7.551	32
17		Si	3.36	12.36	6.368	33.5
18		Str Steel	3.36	13.05	7.096	32

Table 4 — COMSOL Simulated Results in Load Dependence at 31.5 Hz

			Load Dependence			
Device	Material		La Mixing (%)	Voltage (V)	Power (W)	Resistance (k Ω)
1	PZT-5A	Cu	1.12	7.405	2.742	10
2		Si	1.12	8.028	5.731	5.6
3		Str Steel	1.12	8.756	3.833	10
4	PZT-5A	Cu	2.24	7.440	2.772	10
5		Si	2.24	8.141	5.901	5.62
6		Str Steel	2.24	8.852	3.922	10
7	PZT-5A	Cu	3.36	8.791	12.22	3.16
8		Si	3.36	6.921	4.251	5.62
9		Str Steel	3.36	8.012	3.221	10
10	PZT-5J	Cu	1.12	6.750	12.81	1.77
11		Si	1.12	6.698	3.981	5.62
12		Str Steel	1.12	5.960	3.151	5.6
13	PZT-5J	Cu	2.24	7.640	16.41	1.77
14		Si	2.24	6.991	4.351	5.62
15		Str Steel	2.24	6.143	3.352	5.6
16	PZT-5J	Cu	3.36	8.805	12.32	3.16
17		Si	3.36	6.581	3.851	5.6
18		Str Steel	3.36	5.791	2.982	5.62

Overall, this analysis confirms the robustness of the proposed design and its suitability for low-frequency ambient vibrations, where variations in excitation amplitude directly translate into proportional enhancements in electrical power output. In Table 5, the simulated output voltage and electrical power response were observed when the beam was subjected to sinusoidal acceleration from vibration. Between 20 Hz and 32 Hz, a significant increase was observed in voltage and power.

4.4 Electric Potential

Electric potential in piezoelectric materials refers to the voltage developed within the material when it undergoes mechanical deformation or when an external electric field is applied. In the present simulation, PZT-5A devices 3, 6, 9, and the undoped device 19 were evaluated at a resonant frequency of 31.5 Hz, producing maximum electric potentials of 23.7 V, 24.5 V, 25.5 V, and 16.4 V, respectively and values that exceed those reported in earlier studies on ambient structural vibrations[5,8]. Similarly, PZT-5J devices 10, 13, 16, and 22 yielded maximum electric potentials of 14.7 V, 14.9 V, 15.9 V, and 12.3 V at the same resonant frequency. Although the absolute voltage levels for PZT-5J were lower than those of PZT-5A, lanthanum modification consistently

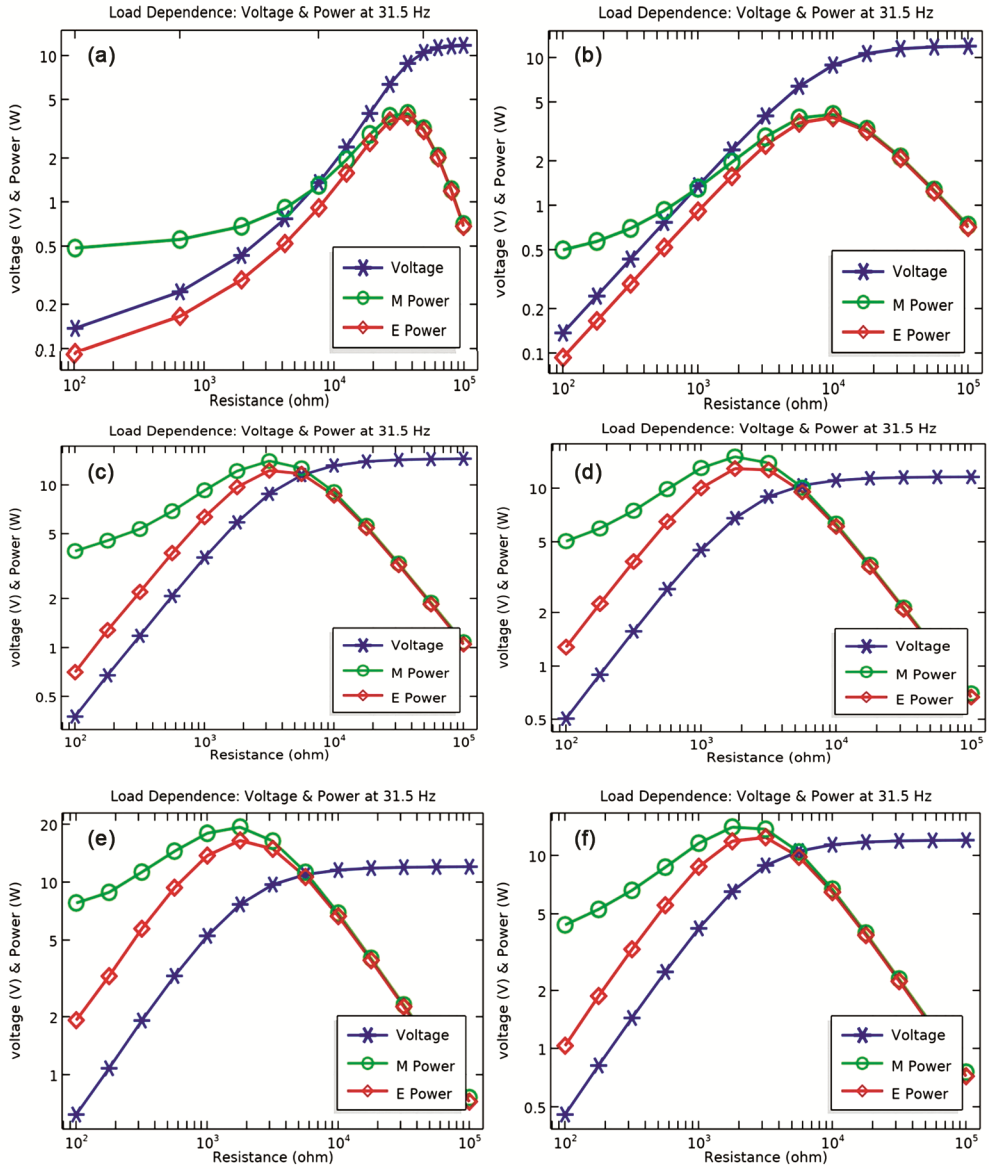

Fig. 3 — Load dependence of devices: In case of PZT -5A with structural steel (a) Device 3 (1.12 % lanthanum) (b) Device 6 (2.24 % lanthanum) (c) Device 9 (3.36 % lanthanum). In case of PZT-5J with copper (d) Device 10 (1.12 % lanthanum) (e) Device 13 (2.24 % lanthanum) and (f) Device 16 (3.36 % lanthanum)

improved the electrical response relative to the undoped configuration. The corresponding electrical power generated under ambient vibration conditions was also evaluated and systematically compared with previous findings, as summarized in Table 5. The combined voltage and power results confirm the effectiveness of lanthanum mixing in enhancing the electromechanical response of PZT-based energy harvesters operating in the low-frequency range.

4.5 Von Mises

The von Mises stress represents the equivalent or effective stress that would produce the same level of deformation or failure as the actual multiaxial stress state when applied uniformly in all directions. In piezoelectric energy harvesters, evaluating von Mises stress is essential to ensure mechanical reliability and safe operation under resonant excitation.

In the present simulation, PZT-5A devices 3, 6, 9, and the undoped device 19 were evaluated at a resonant frequency of 31.5 Hz, yielding maximum von Mises stresses of 2.62×10^8 N/m², 2.85×10^8 N/m², 2.86×10^8 N/m², and 2.70×10^8 N/m², respectively. These results indicate a marginal increase in stress with lanthanum incorporation,

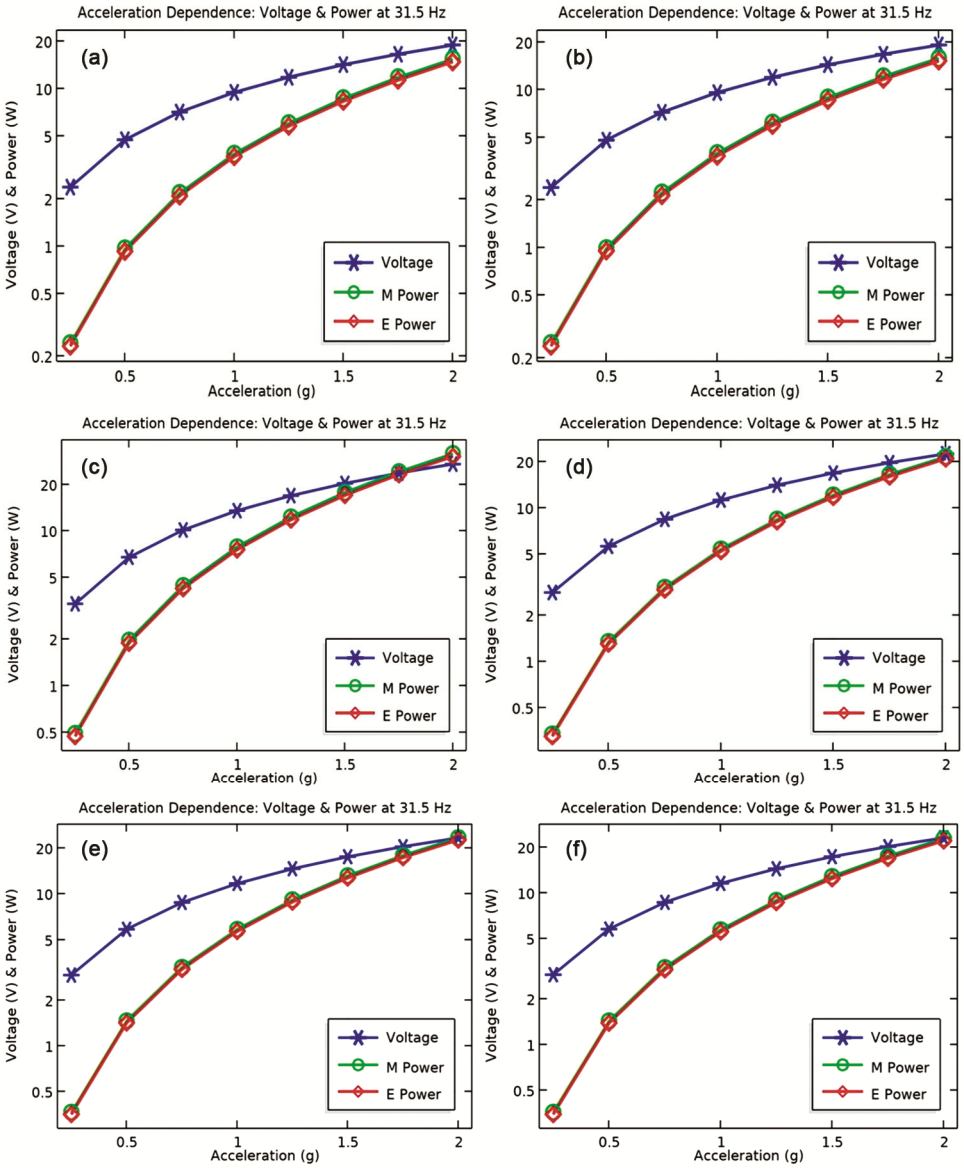

Fig. 4 — Acceleration dependence of devices: In case of PZT -5A with structural steel (a) Device 3(1.12 % lanthanum) (b) Device 6 (2.24 % lanthanum) (c) Device 9 (3.36 % lanthanum). In case of PZT-5J with copper (d) Device 10 (1.12 % lanthanum) (e) Device 13 (2.24 % lanthanum) and (f) Device 16 (3.36 % lanthanum)

attributable to enhanced strain localization near the fixed end of the cantilever.

For PZT-5J, devices 10, 13, 16, and 22 produced maximum stresses of 2.27×10^8 N/m², 2.28×10^8 N/m², 2.45×10^8 N/m², and 2.30×10^8 N/m² under the same excitation conditions. These values indicate that lanthanum mixing does not significantly increase mechanical stress beyond material limits but improves strain-induced electrical output effectively.

Overall, the stress analysis confirms that La mixing enhances the electrical output without introducing excessive von mises stress or compromising structural integrity. This demonstrates that the proposed piezoelectric energy harvester design operates safely within material limits while achieving improved electromechanical performance.

A performance comparison of various piezoelectric energy harvesters from 2019–2025 alongside the present devices is illustrated in Table 6. This highlights variations in piezoelectric materials, substrates, electrode layers, dopant concentration, operating frequency, active volume, and output power. Compared with previous energy harvesters, the present La mixed PZT-5A and PZT-5J based

Table 5 — COMSOL Simulated Results in Acceleration Dependence at 31.5 Hz

Device	Material		Acceleration Dependence			Acceleration (*g*)
			La Mixing (%)	Voltage (*V*)	Power (*W*)	
1		Cu	1.12	16.22	10.9	2
2	PZT-5A	Si	1.12	20.5	17.59	2
3		Str Steel	1.12	18.78	14.7	2
4		Cu	2.24	16.34	11.13	2
5	PZT-5A	Si	2.24	20.94	18.2	2
6		Str Steel	2.24	19.03	15.09	2
7		Cu	3.36	26.85	30.03	2
8	PZT-5A	Si	3.36	19.4	15.69	2
9		Str Steel	3.36	17.49	12.75	2
10		Cu	1.12	22.3	20.73	2
11	PZT-5J	Si	1.12	16.49	11.33	2
12		Str Steel	1.12	16.11	10.8	2
13		Cu	2.24	23.26	22.55	2
14	PZT-5J	Si	2.24	17.07	12.15	2
15		Str Steel	2.24	16.58	11.45	2
16		Cu	3.36	22.98	22.01	2
17	PZT-5J	Si	3.36	16.71	11.63	2
18		Str Steel	3.36	16.16	10.88	2

Table 6 — Performance comparison of various piezoelectric energy harvester

Reference	Year	Piezoelectric material	Substrate	Layer	La Mixing %	Active Volume (mm^3)	(g)	Frequency (Hz)	Power (mW)
[3]	2019	ZnO	ITO/PET	Ag	1-7.5	-	1	1	2.5×10^{-4}
[4]	2023	$BaSnO_3$	MgO	LBSO	3-7	-	1	-	1.8×10^{-4}
[5]	2019	PVDF/BLT	Cu	BLT	1-5	12	0.8	1500	50×10^{-4}
[6]	2019	ZnO	ITO/PET	Ag/PET	5	-	0.9	1500	50×10^{-4}
[8]	2024	PZT 4	Fe/Cr/Ni	-	-	135	1	19	8×10^{-4}
[9]	2024	PVDF / Sr-doped $LaCoO_3$ / MWCNT	PVDF	Composite film	7.5 wt.	-	1	1	0.047
[10]	2024	PVDF / La_2CuMnO_6 / PPy	PVDF	Al / Composite	10 wt.	1.69	-	2	0.0315
[11]	2025	Pr-doped $La_2Ti_2O_7$	Mica	ITO / Al	0.19–0.92	-	-	-	0.0011
[12]	2024	La-doped BNKT-ST	ceramic	Bulk disc	0.03 mol	-	-	-	-
[13]	2024	La, Zr-doped $BiFeO_3$	Bulk ceramic	Bulk disc	10-15 mol	-	-	-	-
[14]	2025	La-doped $PbTiO_3$	Bulk ceramic	Bulk disc	6 wt.	-	-	20×10^3	-
[15]	2025	PLZT	Glass/PET	ITO / PLZT / ITO	9	240	-	5600	-
[16]	2020	PZT	Si	-	-	315	1.2	160	20×10^3
[26]	2022	PZT-4	Si	Pt/Ti	-	1.886	0.07	30	7.156×10^{-3}
[26]	2022	PZT-5A	Si	Pt/Ti	-	1.886	0.07	28.4	8.657×10^{-3}
[26]	2022	PZT-5H	Si	Pt/Ti	-	1.886	0.07	28.6	10.73×10^{-3}
[26]	2022	PZT-8	Si	Pt/Ti	-	1.886	0.07	30.2	5.701×10^{-3}
[27]	2023	PZT-5H	Cu	-	-	-	0.6	64.11	56.3×10^{-3}
Device 1	Present	PZT-5A	Cu	Nickel	1.12	148.96	2	31.5	8.004
Device-2	Present	PZT-5A	Si	Nickel	1.12	148.96	2	33.5	7.469
Device 3	Present	PZT 5A	Str steel	Nickel	1.12	148.96	2	32	9.485
Device-4	Present	PZT-5A	Cu	Nickel	2.24	147.27	2	31.5	8.450
Device-5	Present	PZT-5A	Si	Nickel	2.24	147.27	2	33.5	7.580
Device-6	Present	PZT-5A	Str steel	Nickel	2.24	147.27	2	31.5	9.880
Device-7	Present	PZT-5A	Cu	Nickel	3.36	145.58	2	31.5	7.850
Device-8	Present	PZT-5A	Si	Nickel	3.36	145.58	2	33.5	8.334
Device 9	Present	PZT 5A	Str steel	Nickel	3.36	145.58	2	32	9.983
Device-10	Present	PZT-5J	Cu	Nickel	1.12	148.96	2	32	7.262
Device-11	Present	PZT-5J	Si	Nickel	1.12	148.96	2	33.5	5.874

(*Contd.*)

Table 6 — Performance comparison of various piezoelectric energy harvester — (*Contd*.)

Reference	Year	Piezoelectric material	Substrate	Layer	La Mixing %	Active Volume (mm^3)	(g)	Frequency (Hz)	Power (mW)
Device 12	Present	PZT 5J	Str steel	Nickel	1.12	148.96	2	32	6.536
Device-13	Present	PZT-5J	Cu	Nickel	2.24	147.27	2	32	7.170
Device-14	Present	PZT-5J	Si	Nickel	2.24	147.27	2	33.5	6.220
Device-15	Present	PZT-5J	Str steel	Nickel	2.24	147.27	2	32	7.046
Device-16	Present	PZT-5J	Cu	Nickel	3.36	145.58	2	32	7.550
Device-17	Present	PZT-5J	Si	Nickel	3.36	145.58	2	33.5	6.368
Device 18	Present	PZT 5J	Str steel	Nickel	3.36	145.58	2	32	7.096
Device-19	Present	PZT-5A	Cu	Nickel	0	150.46	2	32	8.540
Device-20	Present	PZT-5A	Si	Nickel	0	150.46	2	33.5	7.330
Device-21	Present	PZT-5A	Str steel	Nickel	0	150.46	2	32	7.810
Device-22	Present	PZT-5J	Cu	Nickel	0	150.46	2	32	7.410
Device-23	Present	PZT-5J	Si	Nickel	0	150.46	2	34	5.388
Device-24	Present	PZT-5J	Str steel	Nickel	0	150.46	2	32.5	6.870

piezoelectric energy harvesters demonstrate substantially higher output power in the low frequency range, indicating improved energy harvesting efficiency and suitability for low ambience vibration applications.

5 Conclusion

This study used coupled finite element simulations and a reduced single-degree-of-freedom electromechanical model to evaluate the influence of La mixing on the performance of serendipity-shaped cantilever piezoelectric energy harvesters based on PZT-5A and PZT-5J. The results demonstrated that the controlled La mixing consistently enhanced the electromechanical coupling, output voltage and harvested power across all substrate configurations. PZT-5A on a structural-steel substrate with 3.36 % La achieved the highest output of 15.47 V and 9.98 mW at 32 Hz, representing an improvement of approximately 12–13% over undoped devices. Mathematical analysis further validated the simulation outcomes, yielding a maximum power of 9.319 mW at 50 kΩ and an extraction efficiency of 26.1%, and a total damping ratio of 0.0135. The computed capacitance for PZT-5A and PZT-5J were 96.2 nF and 107.5 nF, with corresponding capacitive reactance of 51.7 kΩ and 46.3 kΩ at resonance.

These findings confirm that La mixing improves the piezoelectric charge without imposing excessive mechanical stress, making La- mixed PZT a suitable choice for low-frequency vibration harvesting. Future work will involve device fabrication, experimental validation, multi-mode dynamic analyses, and integration with rectification and power management circuits. Overall, the proposed La-mixing is a viable technique for developing compact, efficient piezoelectric harvesters for structural health monitoring and self-powered wireless sensor applications.

Reference

1 Mahapatra S D, Mohapatra P C, Aria A I, Christie G, Mishra Y K, Hofmann S & Thakur V K, *Adv Sci*, 8 (2021) 2100864.

2 Liu H, Zhong J, Lee C, Lee S W & Lin L, *Appl Phys Rev*, 5 (2018) 041306.

3 Rajagopalan P, Jakhar P, Palani I A, Singh V & Kim S J, *Int J Precis Eng Manuf Green Technol*, 7 (2020) 77.

4 Kim H, Kim G, Jeon Y U, Lee W, Lee B H, Kim I S & Kim J, *Adv Sci*, 11 (2024) 2302410.

5 Kim S, Nguyen T M H, He R & Bark C W, *Nanoscale Res Lett*, 16 (2021) 47.

6 Pandey R, Khandelwal G, Palani I A, Singh V & Kim S J, *Nanoscale*, 11 (2019) 14032.

7 Pracucci A, Vandi L, Belletti F, Melo A R A, Vlachos M, Amditis A & Esteves D S, *Energies*, 17 (2024) 1789.

8 Kaur N, Mahesh D & Singamsetty S, *Adv Struct Eng*, 23 (2020) 1010.

9 Shohag S A U, Franco L, Tippur A, Mohan S, Rahman M W & Uddin M J, ACS *Appl Eng Mater*, 2 (2024) 2842.

10 Das T, Yadav M K, Dev A & Kar M, *Chem Eng J*, 496 (2024) 153926.

11 Chabungbam A S, Kim D E, Kim G, Kim M, Lee H S, Kymissis I & Park H H, *J Alloys Compd*, 1011 (2025) 178370.

12 Aly K A, Athikesavan V, Kumar E R & Ebrahium M M, *Ceram Int*, 50 (2024) 11676.

13 Radojković A, Luković-Golić D, Orsini N J, Nikolić N, Ćirković J, Lazarević S & Despotović Ž, *J Alloys Compd*, 1009 (2024) 176901.

14 Serag E N, Altarawneh A M, Hemeda O M, Gawad S A & Salem M M, *Ceram Int*, 52 (1) (2025) 1.

15 Lee Y, Choi H & Jang J, *Sens Actuators A*, 382 (2025) 116087.

16 Elahi H, *Microsyst Technol*, 27 (2021) 2605.

17 Samanta S, Sankaranarayanan V & Sethupathi K, *Vacuum*, 156 (2018) 456.

18 Ahmad M, Ahmad M K, Nafarizal N, Soon C F, Ismail N M A N, Suriani A B & Mamat M H, *Vacuum*, 202 (2022) 111130.

19 Ahmad M, Ahmad M K, Nafarizal N, Soon C F, Suriani A B, Mohamed A & Mamat M H, *Vacuum*, 182 (2020) 109565.
20 Persano L, Camposeo A, Matino F, Wang R, Natarajan T, Li Q & Pisignano D, *Adv Mater*, 36 (2024) 2405363.
21 Mahapatra S D, Mohapatra P C, Aria A I, Christie G, Mishra Y K, Hofmann S & Thakur V K, *Adv Sci*, 8 (2021) 2100864.
22 Li T & Lee P S, *Small Struct*, 3 (2022) 2100128.
23 Narita F & Fox M, *Adv Eng Mater*, 20 (2018) 1700743.
24 Li Z, Roscow J, Khanbareh H, Taylor J, Haswell G & Bowen C, *Mater Today Energy*, 37 (2023) 101396.
25 Hsu T R, MEMS Microsyst, 2nd Edn (John Wiley & Sons, New Jersey), 2020.
26 Debnath B & Kumar R, *IEEE Trans Ind Appl*, 58 (2022) 3901.
27 Kouritem S A, El-Gamal H A & Mohamed K T, *Microsyst Technol*, 29 (2023) 729.